Organic electrochemical transistors manufactured by laser ablation and screen printing

Marzieh Zabihipour[‡1], Per Janson[‡1], Magnus Berggren[1], Daniel T. Simon[1], Peter Andersson Ersman[*2], Isak Engquist[1]

[1] Laboratory of Organic Electronics, Department of Science and Technology, Linköping University, SE-60174 Norrköping, Sweden

[2] RISE Research Institutes of Sweden – Digital Systems – Smart Hardware – Printed, Bio- and Organic Electronics, SE-60117 Norrköping, Sweden

[‡] These authors contributed equally to this work.

[*] Corresponding author: peter.andersson.ersman@ri.se

Abstract

The dimensions of the material serving as the channel in organic electrochemical transistors (OECTs) are important for the overall switching performance. Here, a laser ablation step is included in the OECT manufacturing process, in an attempt to shorten the channel length of the OECT. The source and drain electrodes are formed by laser ablation of a previously screen printed carbon-based rectangle, which in this study resulted in an average channel length equal to 25 μm. All other processing steps rely on screen printing, allowing for large-area manufacturing of OECTs and OECT-based circuits on flexible substrates. This approach results in a manufacturing yield of 89 %; 178 out of a total of 200 OECTs exhibited an ON/OFF ratio exceeding 1000 with a statistical mean value of 28,000 and reproducible switching performance. OECT-based circuits, here demonstrated by a logic inverter, provide a reasonably high voltage gain of 12. The results thus demonstrate another reliable OECT manufacturing process, based on the combination of laser ablation and screen printing.

Introduction

Low-voltage operation in an field effect transistors (FETs)[1–3] requires the dielectric layer between the gate electrode and the channel to be very thin, making such devices highly sensitive to the manufacturing technique, *i.e.*, thin and smooth layers are required in order to provide proper device functionality. In contrast, the electrolytic interfaces used in an organic electrochemical transistor

(OECT)[4–14] enable operation at very low voltages, typically less than 1 V, independent of the electrolyte thickness. This is of critical importance since it allows for device manufacturing via various printing techniques[15–21], despite the deposition of thicker layers at lower resolution and less smoothness. Due to the simple device architecture and low-voltage operation[22,23], the OECT is a versatile device platform that can be used in a wide variety of applications and research fields[3,24–27]. Screen printed OECTs and OECT-based circuits have previously been reported[6,10,11,28,29], and despite being a relatively rough (low resolution) printing technique, screen printing has been shown capable of achieving scalable production of complex logic circuits and OECT arrays. However, screen printing not only provides relatively thick layers, but the lateral resolution of this printing technique also limits the performance of the resulting OECT devices. The limiting factor is mainly the channel lengths achievable by using screen printing, where shorter channels result in higher conductivity in the ON state and lower overall device capacitance. In previous reports, high yield manufacturing of OECTs and OECT-based inverters were achieved using channel lengths in the range 80-200 µm[13,29]. Attempting to screen print OECT channel lengths in the range 50-75 µm, or even shorter, typically results in significantly lower device reproducibility. Previously, Blaudeck, *et al.*[30] reported OECTs that were manufactured with a hybrid manufacturing method based on printing techniques (screen and inkjet printing), patterning of the source and drain electrodes via laser ablation, followed by lamination of the gate electrode on top of a non-cured electrolyte layer. The laser ablation process resulted in OECT channels with large dimensional variations, thereby leading to inconsistent OECT switching performance and low manufacturing yield (20-25 %). This was evidenced by non-symmetric switching times, the OFF-to-ON switching time was approximately a factor of 3 longer as compared to the opposite switching direction, the shortest switching times were 160 ms (ON-to-OFF) and 460 ms (OFF-to-ON), respectively, and the best ON/OFF ratio was ~600.

Here, we seek to achieve shorter channel lengths while maintaining high production yield by using a laser ablation step. Instead of using additive deposition of each layer, as is the case when solely using screen printing, laser ablation is introduced as a subtractive method to remove the middle part of a previously screen printed carbon rectangle, resulting in two separated carbon-based source and drain electrodes. Besides the sole laser ablation processing step, all other layers of the OECTs presented here were deposited via screen printing. Thereby, in this study, 200 OECTs are manufactured to investigate the manufacturing yield of the OECTs together with their electrical switching performance. ON/OFF ratios up to 577,000 and switching times down to 24 ms were obtained for the OECTs. The satisfactory switching time motivated us to include the OECTs in logic inverter circuits to evaluate their behavior upon applying a gate voltage at different frequencies. A voltage gain of ~12 and a propagation delay of 90 ms was achieved for the OECT-based inverters.

Results and Discussion

OECT Fabrication

The current throughput of an OECT is governed by the three-dimensional geometry of the channel: length (L), width (W) and thickness (t), where the channel length is defined as the separation between the source and drain electrodes. Similar to the majority of reported OECTs, the devices presented here rely on poly(3,4-ethylenedioxythiophene) doped with poly(styrene sulfonic acid) (PEDOT:PSS) as the active material in the channel. Since PEDOT:PSS is an electronic conductor in its pristine state, the OECTs are said to be operated in depletion mode, and this also explains why the current throughput depends on the thickness of the channel. In a fully screen printed device, the source and drain electrodes are patterned directly as separate rectangles by the mesh of the screen. Here, a single carbon-based rectangle was patterned by screen printing, and subsequently divided into two regions by the laser ablation process. The width of the laser beam therefore defines the separation distance – the OECT channel length (L) – between the carbon-based source and drain electrodes formed by the ablation step. The OECT channel openings (*i.e.*, the separation between the source and drain electrodes) were formed using the following settings for the laser ablation step: 0.90 W, 80 Hz, 0.0355 m/s travel speed. These settings were chosen to ensure full cutting with minimal damage to the PET substrate beneath, to optimize the formation of the channel length.

Subsequent to the laser ablation step, the remaining OECT layers were screen printed on top of each other (Figure 1). The OECT channel was formed by a PEDOT:PSS layer screen printed between the source and drain carbon pads, with a channel width (W) smaller than the width of the carbon pads. This means that the width of the OECT channel was determined by the width of this PEDOT:PSS layer (~200 µm) and the length of the channel was determined by the laser-patterned spacing between the source and drain electrodes.

PEDOT:PSS deposition was followed by deposition of an insulating layer. The purpose of this layer is to prevent short-circuits and minimize parasitic current contribution from the interfaces between the carbon electrodes and the electrolyte. The electrolyte layer, based on poly(diallyldimethylammonium chloride) dissolved in water, was then screen printed into the area defined by the insulating layer, such that the electrolyte was brought into contact with the PEDOT:PSS-based channel. The electrolyte layer was then solidified via UV-curing. Finally, a PEDOT:PSS-based gate electrode was screen printed onto the electrolyte layer. Silver-based conductors and contact pads were optionally screen printed to minimize the overall resistance of the devices.
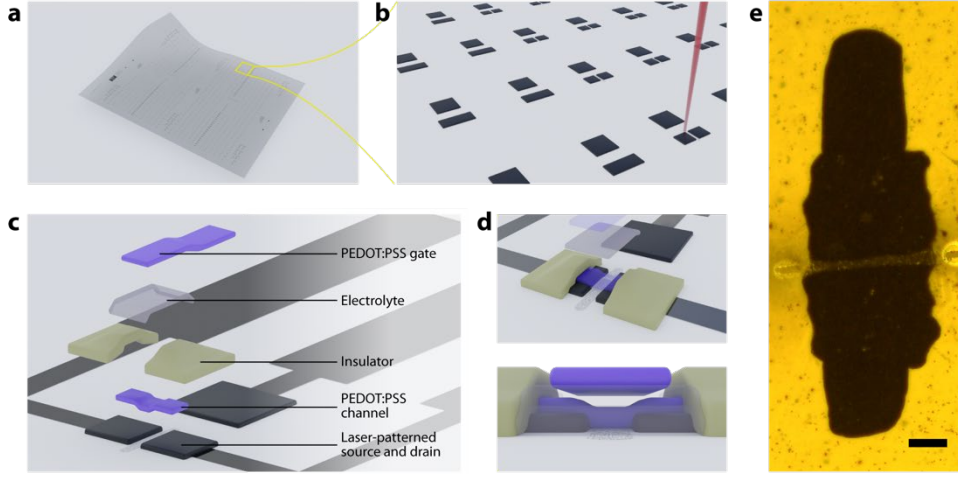
*Figure 1: Large-area manufacturing of OECTs using a combination of laser ablation and screen printing. **a**, The design layout covers an area approximately equal to an A4 sheet. **b**, The laser ablates parts of a previously screen printed carbon-based rectangle, thereby forming the source and drain electrodes. **c**, Exploded view of the various layers of the OECT. **d**, Zoom-in of the active part of the OECT (upper panel) and the cross-sectional view of the OECT architecture (lower panel). **e**, Microscope image of carbon separated by laser ablation, thereby forming an OECT channel length of ~25 µm. Scale bar 100 µm.*

OECT Characterization

The 200 OECTs fabricated on two different PET films were evaluated in terms of transfer and output characteristics. For the transfer characteristics, at a constant drain voltage (V_D) of -1 V, the gate voltage (V_G) was swept from 0 V to 1.5 V with 10 mV steps. While recording the output characteristics of the OECTs, V_D was swept from 0 V to -1.2 V and V_G was subsequently changed from 0 to 1.35 V using a voltage step of 0.15 V. Among the 200 manufactured OECTs, 178 (89 %) OECTs were fully functional. Figure S1 shows the statistical data of the switching performance of the 178 operational OECTs in terms of their ON/OFF ratio, expressed as $\log_{10}(\frac{I_{D,ON}}{I_{D,OFF}})$. We observe that the average and standard deviation of $\log_{10}(\frac{I_{D,ON}}{I_{D,OFF}})$ is 4.33 and 0.26, respectively. An ON/OFF ratio $\left(\frac{I_{D,ON}}{I_{D,OFF}}\right)$ of at least 1,000 was used to define a functional device. Among the 178 functional devices, 167 (94 %) devices exhibited an ON/OFF ratio exceeding 10,000, an average value of the ON/OFF ratio equal to ~28,000 and the highest recorded ON/OFF ratio was 577,000 (Figure S1). Functional OECTs behaved consistently with a drain current (I_D) in the ON state (I_{ON}) of approximately -1.5 mA and an I_D in the OFF state (I_{OFF}) in the approximate range -50 to -100 nA. Figure 2 exemplifies the OECT switching performance, where Figure 2a shows the transfer sweeps of five OECTs and Figure 2b shows the output characteristics for one of these OECTs. The transfer sweeps for the five OECTs in Figure 2a show almost identical I_{ON} and I_{OFF} values, resulting in an ON/OFF ratio exceeding 10,000. It should be noted that the thickness of the screen printed channels is relatively thick (~500 nm). This, combined with that the channels are reduced to their fully depleted states, are the two main reasons for the hysteresis behavior observed

in the transfer sweeps. In the output characteristics presented in Figure 2b (I_D shown in logarithmic scale, Figure S2 shows I_D in linear scale), both the linear and saturation regions are shown.


a

b
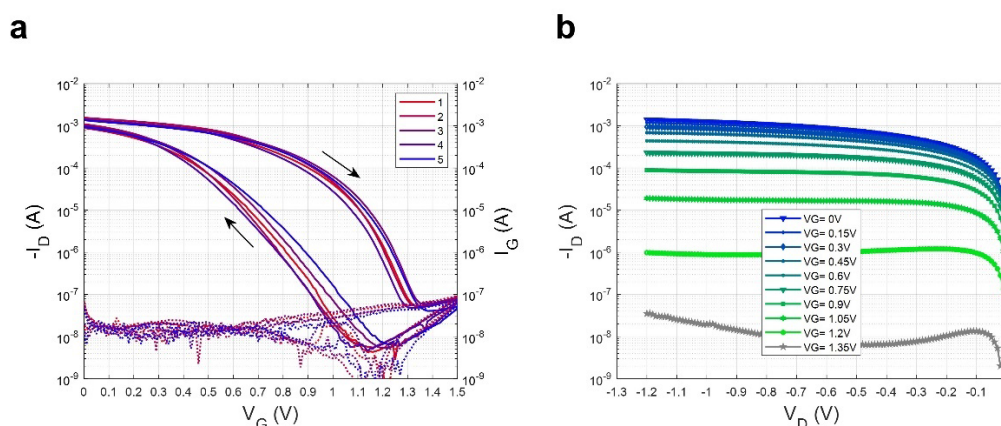
*Figure 2: The graphs illustrate the OECT switching performance. **a,** Transfer sweeps of five OECTs at V_D = -1 V. **b,** Output curves (logarithmic scale) of one of these OECTs at different V_G.*

Furthermore, dynamic switching tests were carried out for some of the OECTs, in which the I_D was recorded upon applying a square wave V_G signal switching between 0 and 1.4 V while simultaneously providing a constant V_D of -1 V. Figure 3 illustrates the dynamic OECT measurements at four different V_G frequencies: 0.1, 0.2, 0.25, and 0.5 Hz. The ON/OFF ratios are in good agreement with those obtained from the transfer and output sweeps shown in Figure 2, i.e., an ON/OFF ratio of at least 10,000 is obtained in all dynamic measurements shown in Figure 3.

The switching time is an important figure of merit which is extracted from the dynamic switching measurements. It is the switching time that determines the switching frequency of OECT-based circuits. Since an ON/OFF ratio of at least 1,000 is used herein to define a functional device, i.e., to estimate the manufacturing yield, we also define the switching time as the time it takes to modulate the drain current by a factor of 1,000. Using this definition, the rise (OFF-to-ON) and the fall (ON-to-OFF) switching time (averaged from the measurements at four different V_G frequencies, see Table S1) is 34 ms and 88 ms, respectively. These switching times agree well previously reported OECTs with screen printed channels[10,13], except that the fall time is longer than the rise time in the devices reported herein. In previous reports, PEDOT:PSS is screen printed directly on the PET substrate to form a smooth and uniform channel, followed by the deposition of the source and drain electrodes. Here, the process is reversed, which may form a thicker channel at the interfaces where PEDOT:PSS is brought in contact with the source and drain electrodes, which in turn prolongs the fall time. Additionally, these switching times are clearly longer than the state of the art OECT performance (~100 μs)[31]. However, the

previously reported data is based on only ~20 % current modulation in miniaturized OECTs, including an aqueous electrolyte with high ion concentration, manufactured by photolithography. Here, the reported switching times are based on much larger current modulation (10^3) obtained in all-printed OECTs including a screen printed electrolyte layer solidified by UV-curing.
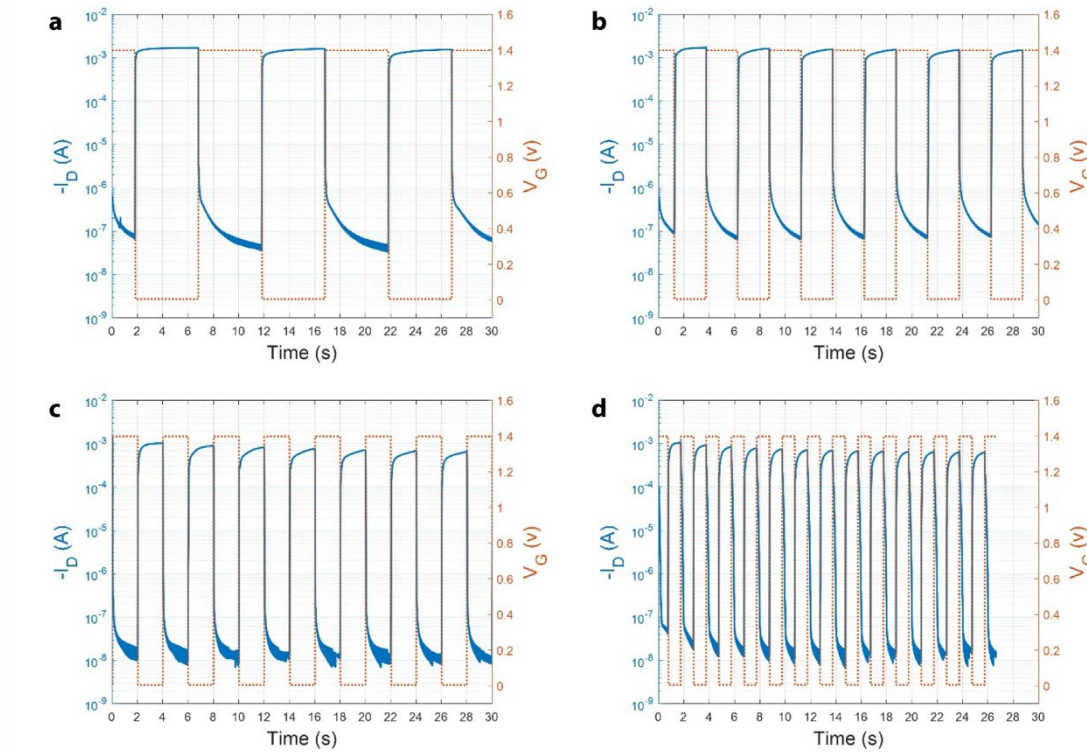

Figure 3: OECT switching behavior in dynamic measurements. A constant V_D of -1 V is applied and V_G switches between 0 and 1.4 V at **a,** 0.1 Hz, **b,** 0.2 Hz, **c,** 0.25 Hz, and **d,** 0.5 Hz.

Inverter Characterization

In the next step, an OECT-based inverter structure was assembled on a breadboard to allow for an evaluation of its switching performance. As shown in Figure 4a, the inverter comprises an OECT and a resistor ladder with three resistors (R_1, R_2, and R_3). The supply voltage of the circuit is connected via two voltage nodes (V_+ and V_-). The output voltage (V_{OUT}) is thus determined by voltage division between the three resistors, V_+, V_-, and the voltage applied to the gate electrode of the OECT (V_{IN}). The V_{IN} levels ($V_{IN,L}$ and $V_{IN,H}$) applied to the gate electrode of the OECT together with the supply voltages and the three resistor values define the V_{OUT} levels ($V_{OUT,L}$ and $V_{OUT,H}$). When $V_{IN,L}$ is applied to the gate electrode, V_{OUT} is determined by V_+, R_1, R_2, and the ON-state channel resistance. When $V_{IN,H}$ instead is applied to the gate electrode, the OECT channel is switched to its high resistance state and the V_{OUT} signal is then governed by V_+, V_-, R_1, R_2, and R_3. Thus, by selecting proper supply voltages and resistor values, the V_{OUT} signal switches between the targeted voltage values. The resistor ladder

employed in this work was R_1 = 442 kΩ, R_2 = 146 kΩ, and R_3 = 316 kΩ, based on experience from our previously published work on OECT inverters[29].
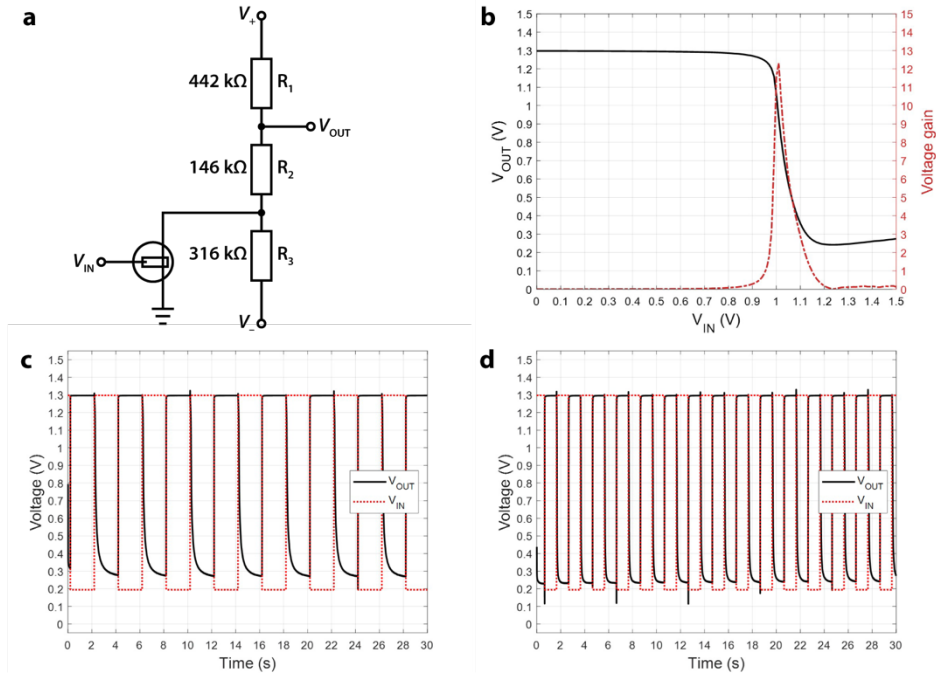
Figure 4: OECT-based inverter circuit. *a, Schematic of the inverter circuit. **b**, Voltage transfer sweep (forward direction) of the inverter circuit including the corresponding voltage gain. **c**, Dynamic switching performance of the inverter, plotted as V_{OUT} vs. time, when V_{IN} switches between 0.2 and 1.3 V at 0.25 Hz and, **d**, 0.5 Hz. V_+ = 5.24 V and V_- = -5.06 V were used as the supply voltage levels.*

The performance of the OECT-based inverter circuit is evaluated with respect to both voltage transfer characteristics and dynamic switching. One approach to evaluate the OECT-based inverter performance in terms of V_{OUT} levels is to observe the voltage transfer characteristics. Figure 4b illustrates a voltage transfer measurement of an inverter in the forward sweep direction, using the supply voltage levels of 5.24 and -5.06 V. Ideally, supply voltage levels of ±5 V were targeted, but a slight adjustment was required due to the minor mismatch between the resistor values in the design and the actual values obtained upon screen printing the resistors.

The voltage gain, defined by the V_{OUT}/V_{IN} ratio, can be extracted from the voltage transfer sweep of the inverter. According to Figure 4b, the obtained voltage gain exceeds 12 when using a set of supply voltages levels of 5.24 and -5.06 V. Hence, the voltage gain value achieved herein is comparable to the value of ~14 recently reported for screen printed OECT-based inverters[29], in which an identical resistor

ladder (R₁=442 kΩ, R₂=146 kΩ, and R₃=316 kΩ) together with an OECT with the channel dimensions of $L{\times}W=80{\times}150$ µm and supply voltage levels of 4.83 and -4.84 V were employed.

In the dynamic switching mode, V_{OUT} is recorded over time when a square wave V_{IN} signal switches between two levels ($V_{IN,L}$ and $V_{IN,H}$), at a specific frequency. Since V_{OUT} relies on voltage division in the inverter circuit, the logic V_{OUT} levels are also dependent on the supply voltage levels for a given set of resistor values in the ladder. Employing different V_{IN} levels thus implies modification of the supply voltage levels. Figure 4c and 4d shows the dynamic switching behavior of the inverter operating at 0.25 and 0.5 Hz, respectively, when V_{IN} switches between 0.2 and 1.3 V and the same supply voltage levels of 5.24 and -5.06 V are applied to the inverter circuit. The motivation of selecting these V_{IN} levels is described in the following: In inverters, by choosing proper supply voltages and resistor values, the V_{OUT} signal switches between the two V_{IN} levels ($V_{IN,L}$ and $V_{IN,H}$). Based on the I–V characteristics of the OECTs in Figure 2a, similar ON current values are found for both V_G = 0 and 0.2 V, hence, the $V_{IN,L}$ level is set to 0.2 V. Besides, as shown in Figure 2a, to switch off the transistor, a $V_{IN,H}$ value of 1.3 V is sufficient. The overall target is to minimize the V_{IN} voltage window, since this implies less voltage strain and thereby prolonged operational lifetime[29]. The V_{OUT} levels achieved in the two independent inverter measurements, the voltage transfer sweep (Figure 4b) and the dynamic switching mode (Figure 4c and 4d), are well matched.

One critical parameter associated with inverters is the propagation delay of the logic signal, which can be extracted from dynamic switching measurements. In general, there is a lag in time from the moment V_{IN} is provided at the input node until the voltage signal has been transmitted to the V_{OUT} node. This propagation delay can be extracted from the rise or fall times of the V_{OUT} signal with respect to half of the amplitude of the V_{IN} window. By using the data in Figure 4, a propagation delay of ~90 ms is obtained for this inverter, independent of the frequency of the V_{IN} signal.

Conclusions

In this study, 200 OECTs were manufactured by a combination of laser ablation and screen printing techniques. Out of the total 200 OECTs, 178 were fully functional and showed consistent switching performance, resulting in a high manufacturing yield of 89 % due to the uniformly patterned/printed structures and layers of these OECTs. The laser ablation process combined with screen printing results in OECTs with reproducible channel dimensions ($L{\times}W{\approx}25{\times}200$ µm), which is evidenced by that all functional OECTs show an ON/OFF ratio exceeding 1,000. The statistical ON/OFF ratio for the 178 operational OECTs shows an average value of ~28,000, which is almost three times higher as compared

to the average ON/OFF ratio recently reported for 600 screen printed OECTs with the channel dimensions of 200×200 μm[13]. Furthermore, the OECTs presented herein show improved switching times (down to 24 ms) as compared previously reported laser ablated OECT devices (>100 ms)[30]. Several OECTs showed an ON/OFF ratio exceeding five orders of magnitude, with a maximum ratio of almost 600,000. Such high ON/OFF ratio is approximately one order of magnitude higher than the recently reported value[29]. The improvements in switching performance are most probably caused by the short channel lengths obtained via the laser ablation step. Additionally, an OECT-based inverter circuit has also been evaluated. This circuit was based on one OECT and a resistor ladder (R_1=442, R_2=146 and R_3=316 kΩ) to enable the intended logic functionality. Dynamic measurements resulted in an inverter propagation delay of 90 ms, while a voltage gain of 12 was extracted from the voltage transfer sweeps. The switching performance of standalone OECTs and OECT-based inverters correlate well with screen printed OECTs, and the results therefore show the feasibility of combining laser ablation and screen printing in the OECT manufacturing process.

Materials and Methods

OECTs are manufactured on polyethylene terephthalate (PET) substrates (*Polifoil Bias* purchased from *Policrom Screen*). The layout of the OECTs was designed in the Clewin software (WieWeb Software Inc., Netherlands). All manufacturing steps were carried out in ambient condition.

The materials of the OECT were deposited by employing a flatbed sheet-fed screen printer (*DEK Horizon 03iX*) with the alignment capability of +/- 25 μm. For the screen printing tools, standard polyester meshes with the mesh counts varying from 75 to 150 threads per cm, and thread diameters ranging from 20 to 50 μm, were utilized. Moreover, the print gap and squeegee pressure altered between 2 and 5 mm and 10 and 20 kg, respectively, and the squeegee angle was ~65°. Silver ink (*Ag 5000* purchased from *DuPont*) consisting of silver flakes was printed on top of the flexible PET substrate to create the contact pads. Subsequently, carbon electrodes (*Du Pont 7102* conducting screen printing paste) were patterned. These layers were thermally treated at 120 °C for 5 min. The substrate was then aligned and processed with a *Speedy 300* industrial engraver (*Trotec Laser GmbH*), fitted with a CO_2 laser (laser power up to 120 W, wavelength 10.6 μm) and mechanics allowing for a traveling speed of maximum 3.55 m/s. The actual cuts were made at 0.0355 m/s and 80 Hz. In the next step, a PEDOT:PSS (*Clevios SV4* purchased from *Heraeus*) stripe was deposited to connect the two carbon source and drain electrodes created by the laser cut, hence, the PEDOT:PSS serves as the electrochemically active transistor channel. This layer was also dried at 120 °C for 5 min. Thereafter, an insulating material (*UVSF* purchased from *Marabu*) was screen printed, followed by UV-curing. This

insulating layer prevents short-circuits and defines the area of the subsequently screen printed electrolyte ink (poly(diallyldimethylammonium chloride) dissolved in water; *E009* provided by *RISE*). The electrolyte layer was UV-cured to transform it into a solid electrolyte layer. Hence, the active channel area of the OECT is defined by the PEDOT:PSS stripe that is in direct contact with the electrolyte layer. Finally, a PEDOT:PSS layer is printed on top of the electrolyte layer, thereby forming the gate electrode.

For the OECT characterization, transfer (I_D vs. V_G), output (I_D vs. V_D), and dynamic switching (I_D vs. time) measurements were carried out using a semiconductor parameter analyzer (*HP/Agilent 4155B*) and a function generator (*Agilent 33120 A*). Inverters were built up using the screen printed OECTs, passive resistors, and a breadboard. For the inverter characterization, the semiconductor parameter analyzer and the function generator were used.

Acknowledgements

References

1.   Torsi, L., Magliulo, M., Manoli, K. & Palazzo, G. Organic field-effect transistor sensors: a tutorial review. *Chem. Soc. Rev.* **42**, 8612–8628 (2013).

2.   Kim, D. W., Min, S.-Y., Lee, Y. & Jeong, U. Transparent Flexible Nanoline Field-Effect Transistor Array with High Integration in a Large Area. *ACS Nano* **14**, 907–918 (2020).

3.   Wadhera, T., Kakkar, D., Wadhwa, G. & Raj, B. Recent Advances and Progress in Development of the Field Effect Transistor Biosensor: A Review. *J. Electron. Mater.* **48**, 7635–7646 (2019).

4.   Shen, H., Abtahi, A., Lussem, B., Boudouris, B. W. & Mei, J. Device Engineering in Organic Electrochemical Transistors toward Multifunctional Applications. *ACS Appl. Electron. Mater.* **3**,

2434–2448 (2021).

5. Méhes, G. *et al.* Organic Microbial Electrochemical Transistor Monitoring Extracellular Electron Transfer. *Adv. Sci.* **7**, 2000641 (2020).

6. Andersson Ersman, P., Nilsson, D., Kawahara, J., Gustafsson, G. & Berggren, M. Fast-switching all-printed organicAndersson Ersman, P., Nilsson, D., Kawahara, J., Gustafsson, G., & Berggren, M. (2013). Fast-switching all-printed organic electrochemical transistors. Organic Electronics, 14(5), 1276–1280. https://doi.org/10.1016/j.orge. *Org. Electron.* **14**, 1276–1280 (2013).

7. Strakosas, X., Bongo, M. & Owens, R. M. The organic electrochemical transistor for biological applications. *J. Appl. Polym. Sci.* **132**, 41735 (2015).

8. Nissa, J., Janson, P., Berggren, M. & Simon, D. T. The Role of Relative Capacitances in Impedance Sensing with Organic Electrochemical Transistors. *Adv. Electron. Mater.* **7**, 2001173 (2021).

9. Nissa, J., Janson, P., Simon, D. T. & Berggren, M. Expanding the understanding of organic electrochemical transistor function. *Appl. Phys. Lett.* **118**, 53301 (2021).

10. Andersson Ersman, P. *et al.* All-printed large-scale integrated circuits based on organic electrochemical transistors. *Nat. Commun.* **10**, 1–9 (2019).

11. Andersson Ersman, P. *et al.* Screen printed digital circuits based on vertical organic electrochemical transistors. *Flex. Print. Electron.* **2**, 45008 (2017).

12. Rivnay, J. *et al.* Organic electrochemical transistors. *Nat. Rev. Mater.* **3**, 17086 (2018).

13. Zabihipour, M. *et al.* High yield manufacturing of fully screen-printed organic electrochemical transistors. *npj Flex. Electron.* **4**, 15 (2020).

14. Diacci, C. *et al.* Real-Time Monitoring of Glucose Export from Isolated Chloroplasts Using an Organic Electrochemical Transistor. *Adv. Mater. Technol.* **5**, 1900262 (2020).

15. Secor, E. B. *et al.* Gravure printing of graphene for large-area flexible electronics. *Adv. Mater.* **26**, 4533–4538 (2014).

16.   Basiricò, L., Cosseddu, P., Fraboni, B. & Bonfiglio, A. Inkjet printing of transparent , flexible , organic transistors. *Thin Solid Films* **520**, 1291–1294 (2011).

17.   Wegener, M. *et al.* Flexographic printing of nanoparticulate tin-doped indium oxide inks on PET foils and glass substrates. *J. Mater. Sci.* **51**, 4588–4600 (2016).

18.   Gaikwad, A. M., Arias, A. C. & Steingart, D. A. Recent Progress on Printed Flexible Batteries: Mechanical Challenges, Printing Technologies, and Future Prospects. *Energy Technol.* **3**, 305–328 (2015).

19.   Faddoul, R., Coppard, R. & Berthelot, T. Inkjet printing of organic electrochemical immunosensors. *Proc. IEEE Sensors* **2014**-**Decem**, 1088–1091 (2014).

20.   Eshkeiti, A. *et al.* Screen Printing of Multilayered Hybrid Printed Circuit Boards on Different Substrates. *IEEE Trans. Components, Packag. Manuf. Technol.* **5**, 415–421 (2015).

21.   Moonen, P. F., Yakimets, I. & Huskens, J. Fabrication of Transistors on Flexible Substrates: from Mass-Printing to High-Resolution Alternative Lithography Strategies. *Adv. Mater.* **24**, 5526–5541 (2012).

22.   Letters, A. P. *et al.* Influence of geometry variations on the response of organic electrochemical transistors. *Appl. Phys. Lett.* **103**, 1–4 (2013).

23.   Hütter, P. C., Fian, A., Gatterer, K. & Stadlober, B. Efficiency of the Switching Process in Organic Electrochemical Transistors. *ACS Appl. Mater. Interfaces* **8**, 14071–14076 (2016).

24.   Leleux, P. *et al.* Organic Electrochemical Transistors for Clinical Applications. *Adv. Healthc. Mater.* **4**, 142–147 (2015).

25.   Braendlein, M., Lonjaret, T., Leleux, P., Badier, J. M. & Malliaras, G. G. Voltage Amplifier Based on Organic Electrochemical Transistor. *Adv. Sci.* **4**, 1600247 (2017).

26.   Liao, J., Si, H., Zhang, X. & Lin, S. Functional Sensing Interfaces of PEDOT:PSS Organic Electrochemical Transistors for Chemical and Biological Sensors: A Mini Review. *Sensors* vol. 19 218 (2019).

27. Keene, S. T. *et al.* Wearable Organic Electrochemical Transistor Patch for Multiplexed Sensing of Calcium and Ammonium Ions from Human Perspiration. *Adv. Healthc. Mater.* **8**, 1901321 (2019).

28. Hütter, P. C., Rothländer, T., Scheipl, G. & Stadlober, B. All Screen-Printed Logic Gates Based on Organic Electrochemical Transistors. **62**, 4231–4236 (2015).

29. Zabihipour, M. *et al.* Designing Inverters Based on Screen Printed Organic Electrochemical Transistors Targeting Low-Voltage and High-Frequency Operation. *Adv. Mater. Technol.* **6**, 2100555 (2021).

30. Blaudeck, T. *et al.* Simplified Large-Area Manufacturing of Organic Electrochemical Transistors Combining Printing and a Self-Aligning Laser Ablation Step. *Adv. Funct. Mater.* **22**, 2939–2948 (2012).

31. Khodagholy, D. *et al.* High speed and high density organic electrochemical transistor arrays. *Appl. Phys. Lett.* **99**, 99–102 (2011).